6-27-2018

Blocking NMDAR Disrupts Spike Timing and Decouples Monkey Prefrontal Circuits: Implications for Activity-Dependent Disconnection in Schizophrenia

Jennifer L. Zick

Rachael K. Blackman

David A. Crowe

Bagrat Amirikian

Adele L. DeNicola

See next page for additional authors

Authors

Jennifer L. Zick, Rachael K. Blackman, David A. Crowe, Bagrat Amirikian, Adele L. DeNicola, Theoden I. Netoff, and Matthew V. Chafee

Published in final edited form as:

Neuron. 2018 June 27; 98(6): 1243–1255.e5. doi:10.1016/j.neuron.2018.05.010.

Blocking NMDAR Disrupts Spike Timing and Decouples Monkey Prefrontal Circuits: Implications for Activity-Dependent Disconnection in Schizophrenia

Jennifer L. Zick[1,2,8], **Rachael K. Blackman**[1,2,7,8], **David A. Crowe**[5], **Bagrat Amirikian**[1,3,4], **Adele L. DeNicola**[1,4], **Theoden I. Netoff**[6,9], and **Matthew V. Chafee**[1,3,4,9,10,*]

[1]Department of Neuroscience, University of Minnesota, Minneapolis, MN 55455, USA

[2]Medical Scientist Training Program (MD/PhD), University of Minnesota, Minneapolis, MN 55455, USA

[3]Center for Cognitive Sciences, University of Minnesota, Minneapolis, MN 55455, USA

[4]Brain Sciences Center, VA Medical Center, Minneapolis, MN 55417, USA

[*]Correspondence: chafe001@umn.edu.

AUTHOR CONTRIBUTIONS

Conceptualization, J.L.Z., R.K.B., T.I.N., and M.V.C.; Methodology, J.L.Z., R.K.B., T.I.N., and M.V.C.; Software, J.L.Z., R.K.B., D.A.C., B.A., and M.V.C.; Validation, J.L.Z., D.A.C, and M.V.C.; Formal Analysis, J.L.Z., D.A.C., B.A., T.I.N., and M.V.C.; Investigation, R.K.B., A.L.D., and M.V.C.; Writing–Original Draft, J.L.Z., R.K.B., and M.V.C. (primary); Writing–Review & Editing, J.L.Z., R.K.B., D.A.C., B.A., A.L.D., T.I.N., and M.V.C.; Visualization, M.V.C; Supervision, T.I.N. and M.V.C.

STAR★METHODS

Detailed methods are provided in the online version of this paper and include the following:

- KEY RESOURCES TABLE
- CONTACT FOR REAGENT AND RESOURCE SHARING
- EXPERIMENTAL MODEL AND SUBJECT DETAILS
  - Monkeys
- METHOD DETAILS
  - Surgery
  - Behavioral task
  - Experimental conditions
  - Neural recording
- QUANTIFICATION AND STATISTICAL ANALYSIS
  - Artifact removal
  - Cross-correlation analyses
  - Trial time resolved cross-correlation analysis
  - Transfer entropy
  - Relation between neural signaling and functional coupling
- DATA AND SOFTWARE AVAILABILITY

SUPPLEMENTAL INFORMATION

Supplemental Information includes eight figures and can be found with this article online at https://doi.org/10.1016/j.neuron.2018.05.010.

DECLARATION OF INTERESTS

The authors declare no competing interests.

[5]Department of Biology, Augsburg University, Minneapolis, MN 55454, USA

[6]Department of Biomedical Engineering, University of Minnesota, Minneapolis, MN, 55455 USA

[7]Present address: Department of Psychiatry and Human Behavior, Alpert Medical School of Brown University, Providence, RI 02906, USA

[8]These authors contributed equally

[9]Senior author

[10]Lead Contact

SUMMARY

We employed multi-electrode array recording to evaluate the influence of NMDA receptors (NMDAR) on spike-timing dynamics in prefrontal networks of monkeys as they performed a cognitive control task measuring specific deficits in schizophrenia. Systemic, periodic administration of an NMDAR antagonist (phencyclidine) reduced the prevalence and strength of synchronous (0-lag) spike correlation in simultaneously recorded neuron pairs. We employed transfer entropy analysis to measure effective connectivity between prefrontal neurons at lags consistent with monosynaptic interactions and found that effective connectivity was persistently reduced following exposure to the NMDAR antagonist. These results suggest that a disruption of spike timing and effective connectivity might be interrelated factors in pathogenesis, supporting an activity-dependent disconnection theory of schizophrenia. In this theory, disruption of NMDAR synaptic function leads to dys-regulated timing of action potentials in prefrontal networks, accelerating synaptic disconnection through a spike-timing-dependent mechanism.

In Brief

Zick et al. report that blocking NMDAR reduces 0-lag spike correlation and persistently reduces functional coupling between neurons in monkey prefrontal local circuits. NMDAR synaptic dysfunction in schizophrenia could similarly disrupt spike timing and disconnect prefrontal circuits via an activity-dependent process.

INTRODUCTION

Schizophrenia is a disease that presents with positive and negative symptoms late in adolescence or early adulthood, but despite intensive research, the mechanisms of pathogenesis remain largely unknown (Insel, 2010). Separate lines of investigation have provided evidence that schizophrenia produces deficits in cognition (Owen et al., 2016), involves mutations that affect synaptic communication, particularly by NMDA receptors (Fromer et al., 2014; Kirov et al., 2012; Timms et al., 2013), and results in the disconnection of prefrontal networks (Camchong et al., 2011; Glantz and Lewis, 2000; Kang et al., 2011; Kolluri et al., 2005). However, it is not known whether or how these variables may be linked in schizophrenia pathogenesis.

To investigate that question in this study, we (1) trained monkeys to perform a cognitive control task that measures specific deficits in schizophrenia (Barch et al., 2003; Carter et al.,

2012; Jones et al., 2010; MacDonald et al., 2005; MacDonald et al., 2003), (2) administered drugs that block NMDA receptors to mimic some aspects of synaptic dysfunction in schizophrenia (Kirov et al., 2012; Timms et al., 2013; Umbricht et al., 2000), as well as to replicate the same pattern of cognitive control errors in monkeys that has been reported in patients (Blackman et al., 2013; Jones et al., 2010; MacDonald, 2008; MacDonald et al., 2005; MacDonald and Chafee, 2006), and (3) carried out multi-electrode recording in prefrontal cortex of monkeys to characterize how an NMDAR synaptic deficit distorted the spiking dynamics of prefrontal cortical circuits. This allowed us to test the hypothesis that changes in synaptic function, cognitive function, and network connectivity might be linked by an underlying defect in the relative timing with which prefrontal neurons generate action potentials with respect to one another.

We applied cross correlation and transfer entropy (Garofalo et al., 2009; Ito et al., 2011; Schreiber, 2000; Wibral et al., 2013) analyses to quantify functional connectivity between neurons based on the relative timing of their action potentials. We found that blocking NMDAR (1) reduced the frequency with which pairs of prefrontal neurons generated action potentials synchronously (at 0-lag), and (2) persistently disconnected prefrontal circuits, as indicated by the reduction both in the prevalence and strength of functional coupling between prefrontal neurons that outlasted the period of acute NMDAR blockade. This supports a causal theory of schizophrenia in which a distortion of spike timing occurs early in the disease, and drives the subsequent disconnection of prefrontal networks by a spike-timing-dependent, Hebbian process. We refer to this as *activity-dependent disconnection*, and it is closely related to several pre-existing theories of schizophrenia focusing on disrupted synchrony and disconnection in the disease (Friston, 1999; Uhlhaas and Singer, 2015). We presently investigate whether these two aspects of schizophrenia may be associated by investigating their relationship in an animal model.

Prior neural recording studies in monkey prefrontal cortex have characterized how blocking NMDAR alters physiological signals in prefrontal neurons related to working memory and executive control. Blocking NMDAR weakens delay period activity associated with working memory (Wang et al., 2013), reduces the strength and task selectivity of neural signals reflecting executive control in rule-based tasks (Ma et al., 2015; Skoblenick and Everling, 2012), and modifies prefrontal oscillations reflecting trial outcome (Skoblenick et al., 2016). However, prior studies have not investigated how blocking NMDAR alters spike timing in monkey prefrontal circuits or whether such a change in spiking dynamics may persistently decouple prefrontal circuits. Here, we report that reducing NMDAR-mediated synaptic transmission disrupts spike timing in prefrontal circuits in a way that could lead to the activity-dependent synaptic disconnection of these circuits over time, potentially linking synchrony and connectivity deficits in the disease.

RESULTS

We recorded the spiking patterns of individual neurons in ensembles of ~15–30 simultaneously recorded neurons in dorsolateral prefrontal cortex (Brodmann area 46; Figures 1E and 1F) of two male rhesus macaque monkeys as they performed a continuous performance task (dot-pattern expectancy, DPX) (Figures 1A–1D). The DPX task (Jones et

al., 2010) is a variant of the AX continuous performance task (AX-CPT) that reveals specific deficits in cognitive control in patients with schizophrenia as well as their first-degree relatives (Barch et al., 2003; Jones et al., 2010; MacDonald, 2008; MacDonald et al., 2003, 2005). We compared the spiking dynamics of prefrontal neural ensembles under three experimental conditions: (1) drug naive, (2) saline, (3) and drug. In the drug naive condition, we characterized prefrontal spiking dynamics before monkeys had received their first injection of phencyclidine (PCP). (On a subset of drug naive days, monkeys received a saline injection to control for the stress of injection). Once drug naive data collection was complete, we began a regimen in which single drug (drug condition) and saline (saline condition) injections were administered on interleaved days, and neural recording in prefrontal cortex was conducted for several hours following the daily injections (see Figure S1 for a schedule of drug and saline injections administered in conjunction with neural recording in each monkey.) We compare the spiking dynamics of prefrontal ensembles across these three conditions. We have previously reported that blocking NMDAR in monkeys with ketamine induces a transient deficit in cognitive control during which they commit a trial-type-specific error pattern in the DPX task (Blackman et al., 2013) that closely resembles the trial-type-specific error pattern seen in patients with schizophrenia performing the DPX and AX-CPT (Barch et al., 2003; Jones et al., 2010; MacDonald, 2008; MacDonald et al., 2003, 2005). The utility of this parallel in behavior between patients with schizophrenia and an animal model performing the same cognitive control tasks is that it may offer a way to investigate changes in prefrontal function at the cellular level using the animal model that could be taking place in the human disease (Averbeck and Chafee, 2016). That parallel, in turn, provides a strategy to identify a class of pathogenic mechanisms that could potentially contribute to disease progression in patients but require investigating prefrontal function at a cellular level to resolve.

In the DPX task, monkeys view a cue followed by a probe stimulus (Figures 1A and 1B) and then move a joystick either to the left or right depending on the cue and probe presented. Cue (Figure 1C) and probe (Figure 1D) stimuli were dot patterns presented on a video monitor during fixation of a central gaze target. One cue dot pattern was designated the A-cue, and 5 alternative dot patterns were collectively designated B-cues (Figure 1C). Similarly, one probe dot pattern was designated the X-probe, whereas 5 alternative dot patterns were collectively designated Y-probes (Figure 1D). On 69% of trials, the A-cue was followed by the X-probe (AX trials). This was the target sequence requiring a target response (leftward movement of the joystick). All other combinations of cues and probes were nontarget sequences that required a nontarget response (rightward movement of the joystick; BX: 12.5%, AY: 12.5%, BY: 6%). The preponderance of AX trials established a prepotent motor habit to move the joystick to the left (target response) whenever the X-probe appears. On BX trials, when the X-probe appears, cognitive control must utilize information about the B-cue stored in working memory to override the prepotent left (target) response typically required to the X-probe and move the joystick to the right (nontarget response) instead. Both patients with schizophrenia (Barch et al., 2003; Jones et al., 2010; MacDonald, 2008; MacDonald et al., 2005), and monkeys following administration of NMDAR antagonists (Blackman et al., 2013) (Figure 1G), make more errors on “BX” trials, releasing

the habitual target response to the X-probe and failing to override this response based on the prohibitive B-cue stored in working memory.

Functional imaging in patients with schizophrenia has reported reduced activation of prefrontal cortex on BX trials relative to healthy controls (MacDonald et al., 2005). In monkeys, prefrontal neuronal responses in the DPX task are strongly biased toward B-cues that require countermanding the habitual (target) response to the X-probe (Blackman et al., 2016). Prefrontal neuronal responses are also augmented following Y-probes that countermand the habitual target response to preceding A-cues (Blackman et al., 2016). At the behavioral level, the elevated BX error rate evident both in patients with schizophrenia and monkeys given NMDAR antagonists could reflect a basic defect in working memory, and working memory deficits in schizophrenia have been extensively documented (Barch and Ceaser, 2012; Goldman-Rakic, 1999; Schwarz et al., 2016). However, the evidence from neural recording in monkeys suggests that prefrontal working memory functions are particularly engaged when the contents of working memory countermand habitual responses (suggesting a specific involvement in cognitive control).

Blocking NMDAR Reduces Synchronous Spiking in Prefrontal Ensembles

We first evaluated the effect of reducing NMDAR synaptic function on the temporal dynamics of spiking between neurons in prefrontal ensembles by computing cross-correlation histograms (CCHs) to quantify the distribution of intervals between spikes in simultaneously recorded neurons (Perkel et al., 1967). CCHs for many individual neuron pairs exhibited a prominent peak at 0-lag (±1 ms; Figure 2A), and in the population, average CCH 0-lag spiking was the dominant pattern (Figure 2C). (Figure S2 provides the distribution of raw synchronous spike rates across all neuron pairs; Figure S3 illustrates the relationship between mean firing rate and synchronous spike rate across all neuron pairs.) To determine whether the 0-lag peak was significant in each neuron pair, we generated a bootstrap distribution of 100 CCHs after randomly jittering the time of each spike within a ±30-ms window. This removed precise spike timing relationships but maintained slower overall fluctuations in mean firing rate. We considered 0-lag peaks significant if they exceeded the 99th percentile of the bootstrap distribution of 0-lag peaks computed from the spike-jittered data.

We compared the prevalence and strength of synchronous spiking in prefrontal cortex across experimental conditions. We found that blocking NMDAR reduced 0-lag spike synchrony in neuron pairs. Administration of NMDAR antagonist significantly reduced both the percent of neuron pairs exhibiting a significant 0-lag peak (Figure 2B, red), and the height of the 0-lag peak (Figures 2C and 2D, red) relative to the saline condition (Figures 2B–2D, blue). These changes in synchronous spiking were not attributable to changes in mean firing rate—we found no significant differences in mean rate across experimental condition (Figure 2E, see legend for statistics). In addition, we found that both the prevalence and strength of 0-lag spiking was significantly reduced in the saline condition (Figures 2B and 2D, blue) relative to the drug-naive condition (black). Because saline and PCP injections were interleaved, reduction in synchronous spiking on saline days following drug days suggests that exposure to PCP produced persistent changes in the spiking dynamics of prefrontal networks. We

found some evidence that these effects were cumulative. The median 0-lag peak height for neuron pairs recorded in the saline condition progressively declined as a function of cumulative NMDAR antagonist exposure, reflecting the number of preceding days that phencyclidine had been injected at a dose of 0.20–0.30 mg/kg (Figure S4). We examine these persistent effects in greater detail below (Figures 4, 5, and 6).

Considering the two monkeys individually, both exhibited the same order of median 0-lag CCH peak amplitude across experimental conditions (Figures S5A and S5B): naive > saline > drug. In addition, 0-lag spike synchrony was modulated with a similar time course in the two monkeys throughout the DPX trial, peaking around the time of the motor response (Figures S5C and S5D). Overall, 0-lag spike correlation was weaker in Monkey 2 than Monkey 1 (Figure S5). Considered individually, the differences in median 0-lag peak height were significant across experimental conditions in Monkey 1, and trended in the same direction in Monkey 2 (Figures S5A and S5B). Combining the 89 ensembles across both monkeys improved the sensitivity of the analysis. For example, the reduction in the median 0-lag peak amplitude between the saline and naive conditions was a trend in both monkeys considered individually (Figures S5A and S5B) but became significant when the data were combined (Figure 2D).

These data provide evidence that blocking NMDARs reduces 0-lag spike synchrony in prefrontal networks, suggesting that the synaptic actions of NMDARs contribute to 0-lag spike synchrony in these networks under normal conditions.

To examine the influence of NMDARs on the variability in spike counts over time, we computed the Fano factor (variance divided by the mean) using the bin-wise spike counts of all recorded neurons. Blocking NMDAR significantly reduced the median Fano factor in the drug condition (Figures 3A–3C, red), relative either to the saline condition (Figures 3A and 3C, blue) or the drug-naive condition (Figures 3B and C, open bars and black), indicating reduced variance in spike counts over bins relative to the mean. The Fano factor did not differ significantly between the drug-naive condition and the saline condition (Figure 3C). The reduction in variance relative to the mean observed to result from NMDAR blockade suggests that prefrontal circuits were less strongly modulated by inputs (resulting in reduced variance in spike rate over time).

The Rate of Synchronous Spiking Was Modulated during Task Performance

We next addressed how spike correlation varied over time in relation to behavior within the DPX task (Figure 4). To factor out the influence of stimulus- and response-driven changes in firing rate on spike correlation, we restricted the analysis to correctly performed AX trials, the condition with the most trials. For each pair of neurons, we computed trial-averaged correlation between a spike occurring in a reference neuron at time t and the spike occurring in a test neuron after a delay τ, at the time $t + \tau$ (see STAR Methods for details). The correlation measure was normalized (Pearson) in such a way that the correlation is zero if the pair fired spikes at times t and $t + \tau$ independently, irrespective of the observed spike rates in the reference and test neurons. Otherwise, it is bound between −1 (fully anti-correlated spiking) and +1 (fully correlated spiking). The resolution of time t describing the point in time during the task was fixed at 50 ms, whereas the spike timing resolution τ was

fixed at 1 ms. Heatmaps in Figure 4 provide the results of this analysis averaged over all recorded neuron pairs and illustrate how spike correlation varied as a function of lag between the spike trains of the two neurons in each pair (y axis) and time in the DPX trial (x axis). Spike trains of the reference neuron were aligned to cue onset each trial. Correlation data are plotted separately for the drug-naive (Figure 4A), saline (Figure 4B), and drug (Figure 4C) conditions.

In all experimental conditions, the temporal relationship between spiking in pairs of prefrontal neurons was dominated by joint spiking at 0-lag (horizontal band of warmer color). Zero-lag spike correlation was strongly modulated during the trial — it increased just before the motor response (that occurred on average near the end of the probe period) and continued for an extended period into the inter-trial interval (Figures 4A–4C and 4H). Population average spike density functions (SDF) are superimposed for comparison (Figures 4A–4C, SDF in white). Changes in mean firing rate and 0-lag correlation were not tightly coupled. For example, in the drug-naive condition, the peak in population firing rate that occurred in the probe and response periods (Figure 4A, SDF) was shifted earlier relative to the peak in 0-lag spike correlation (Figure 4A, band of warm color at 0-lag). In addition, in the drug condition, the increase in population firing rate that occurred during the cue period (Figure 4C; peak in SDF) was not accompanied by an increase in 0-lag spike correlation (note absence of warmer colors in the correlation plot during the cue period). This suggests that to a degree correlated spiking activity and firing rate were modulated during the task rather independently.

We found that blocking NMDAR reduced 0-lag spike correlations between prefrontal neurons. This is evident in the time-resolved spike correlation plots as lighter and cooler shades indicating weaker correlations at 0-lag in the drug condition (Figure 4C) in comparison to the drug-naive condition (Figure 4A) and the saline condition (Figure 4B; note a band of lighter color at 0-lag that is present in the saline condition during the cue and delay periods but is absent from the drug condition). To quantify these effects, we averaged the 0-lag spike correlation values over trial time (Figures 4D–4F), reproducing essential features of the results obtained by the spike-jitter corrected CCH analysis (Figure 2C). Contrasting the populations of neuron pairs in each experimental condition, 0-lag correlations were weaker on average in the drug condition (Figure 4D, red) in comparison to both the saline condition (Figure 4D, blue; Kolmogorov-Smirnov test; $p < 10^{-14}$) and the drug-naive condition (Figure 4D, black; $p < 10^{-41}$). In addition, 0-lag correlations in the saline condition (Figure 4D, blue) were weaker in comparison to the drug-naive condition (Figure 4D, black; $p < 10^{-4}$). Importantly, trial shuffling destroyed 0-lag spike correlations in all experimental conditions (Figure 4F), demonstrating that 1-ms precise spike synchrony detected in simultaneously recorded spike trains is not spurious (i.e., it cannot be simply explained by the lack of enough trials resulting in inaccurate estimation due to the strong fluctuations in the task driven spike rates). Although 0-lag was by far the dominant temporal relationship in joint-spiking (Figure 4D), weaker spike correlations at nonzero lags that considerably exceeded the magnitude of those in trial shuffled spike trains were detected by this analysis as well (Figures 4E and4F, nonzero lags). We explore nonzero lag spike interactions in greater detail by analyzing transfer entropy below (Figure 5).

To determine whether the strength of 0-lag spike correlation varied as a function of behavioral outcome, we contrasted time-resolved spike correlation on correct and error trials (Figure S6). We found that 0-lag spike correlation was significantly weaker on error trials in comparison to correct trials in each experimental condition (see legend to Figure S6 for statistics).

Blocking NMDAR Is Associated with the Persistent Disconnection of Prefrontal Local Circuits

0-lag synchronous spiking could be generated physiologically either by common input or by reciprocal excitatory circuits within prefrontal cortex (Amit and Brunel, 1997; Korndörfer et al., 2017; Pipa and Munk, 2011). In addition to these synchronous dynamics, monosynaptic and polysynaptic communication between neurons in prefrontal local circuits would result in time-lagged spike correlation. To examine such delayed interactions in prefrontal circuits in more detail, we performed transfer entropy (TE) analyses (Garofalo et al., 2009; Ito et al., 2011; Schreiber, 2000; Wibral et al., 2013) (Figure 5). Transfer entropy is an information-theoretic measure (Schreiber 2000) that evaluates the causal relationship between two processes, X and Y, using their observed time series. In our application, TE is a measure of information flow from neuron X to neuron Y obtained from the timing of their respective spike trains. It quantifies in units of bits of information about the future of spiking activity of neuron Y that the past activity of neuron X can provide in addition to the information provided by the past activity of neuron Y alone. We computed TE using an open source toolbox (Ito et al., 2011) over a range of lags from 1 to 10 ms. Naive estimation of information-theoretic quantities from limited experimental samples results in positive bias (Panzeri et al., 2007). We bias-corrected the original TE values at each lag by subtracting the mean of a bootstrap distribution of TE values at the same lag computed using spike trains in which we randomly jittered the time of each spike by ±30 ms. For each neuron pair, we identified the peak TE value across lags. The distribution of the lags at which TE peaks occurred was skewed toward lags under 10 ms (Figure 5C), broadly consistent with functional interactions between neurons at mono- or di-synaptic timescales. We considered neuron pairs to be significantly coupled if the amplitude of the peak TE value exceeded the 99.9^{th} percentile of the bootstrap distribution of all TE peaks across all lags computed using spike-jittered data.

We found evidence that periodic pharmacological blockade of NMDAR persistently disconnected prefrontal networks. The prevalence of significant TE coupling between neurons (Figure 5B), as well as the strength of that coupling measured by the amplitude of the TE peak (Figure 5D) was significantly reduced in both the drug and the saline conditions relative to the drug-naive condition. We found no significant difference in lagged functional coupling between saline and drug conditions (Figures 5B and 5D). These data suggest that blocking NMDAR-mediated synaptic transmission on drug days had a lasting effect on prefrontal circuits by reducing both the strength and prevalence of functional coupling between neurons that persisted on saline days.

To confirm that persistent reduction in spike synchrony and functional coupling on saline days was not attributable to the saline injection itself, we subdivided the neural recording

data obtained before monkeys had received their first injection of phencyclidine (the “naive” experimental condition in Figures 1, 2, 3, 4, and 5) into days that no injection was given (Figure 6, “No injection,” gray) and days that saline was injected (Figure 6, “Saline before drug,” dark blue). (See Figure S1 for the schedule with which these conditions were administered in each monkey.) A comparison between the “No injection” and “Saline before drug” conditions factors out the influence of the saline injection itself on spike synchrony or functional coupling in prefrontal cortex. Saline injections on their own did not significantly influence the amplitude either of the 0-lag CCH peak (Figure 6A) or the lagged TE peak (Figure 6B), comparing the “Saline before drug” data (dark blue) to the “No injection” data (gray). A comparison between “Saline before drug” and “Saline after drug” conditions isolates persistent changes in spike synchrony and functional coupling observed following first exposure to phencyclidine. We found that the amplitude of both the 0-lag CCH peak and lagged TE peaks were significantly reduced in the “Saline after drug” data (Figures 6A and 6B, light blue) relative to the “Saline before drug” data (dark blue). These data support the hypothesis that exposure to phencyclidine induced a persistent reduction both in 0-lag spike synchrony and lagged functional interactions in prefrontal networks.

Patterns of Functional Coupling between Neurons Reflect Their Roles in Information Processing in the DPX Task

We evaluated whether the pattern of functional coupling between neurons reflected the functional properties of neurons defined by their preferences for stimuli and responses in the DPX task and their patterns of firing rate modulation during behavior. Toward that end, we identified two broad activity classes of neurons activated during the DPX task (Figures 7A and 7B), using a simplification of the classification in our prior report (Blackman et al., 2016). Neurons in class I were “switch” neurons that exhibited a preference for B-cues early in the trial (during the cue period) and A-cues late in the trial (during the probe period) (Figure 7A). Switch neurons were the dominant class in prefrontal cortex during DPX performance (Blackman et al., 2016). In contrast, neurons in class II lacked a prominent response to the cue. Instead, their activity ramped up during the probe period and peaked around the time of the motor response (Figure 7B).

To evaluate the relationship between functional coupling and the physiological properties of neurons, we defined “like pairs” as those in which both neurons belonged to the same physiological class (either both neurons in class I or II), and “unlike pairs” as those in which one neuron belonged to class I and the other to class II. We then compared the percent of like and unlike neuron pairs that were significantly coupled either at 0-lag (using CCH analysis), or at nonzero lags (using TE analysis). Differences in coupling probability between like and unlike pairs quantifies a relationship between functional coupling and the physiological classes of neurons, which we term the coupling bias.

We found a significant coupling bias, both with respect to 0-lag interactions based on CCH analysis (Figure 7C) and with respect to lagged interactions based on TE analysis (Figure 7D). Considering 0-lag CCH interactions, a significantly larger proportion of “unlike pairs” than “like pairs” were significantly coupled (Figure 7C). Considering lagged TE interactions, the pattern was reversed, and a significantly larger proportion of “like pairs”

than “unlike pairs” was significantly coupled (Figure 7D). Interactions between prefrontal neurons at different lags therefore varied as a function of the types of information they encoded during behavior. This provides evidence that the pattern of functional coupling between neurons reflected the roles they played in computations performed during behavior, and consequently, the analyses of spike timing we employed captured functional aspects of prefrontal circuit organization.

To evaluate whether blocking NMDAR influenced the pattern of functional interaction between prefrontal neurons (in addition to the strength of those interactions), we defined the condition effect on coupling to be the difference in coupling bias between experimental conditions (naive versus drug, naive versus saline, saline versus drug). None of the condition effects on coupling reached significance (Figure S7; see legend for statistics). Blocking NMDAR appeared therefore to weaken functional interactions between neurons overall but not significantly change the relationship between neuron functional coupling and physiological class.

DISCUSSION

In this study, we investigated how synaptic communication mediated by NMDA receptors influences the temporal dynamics of spiking in monkey prefrontal cortical circuits. Prior studies in monkeys have described local field potentials in prefrontal cortex during AX-CPT performance (Dias et al., 2006) and investigated how blocking NMDAR influences prefrontal oscillatory rhythms (Skoblenick et al., 2016) as well as encoding of behavioral information by individual prefrontal neurons related to working memory (Wang and Arnsten, 2015; Wang et al., 2013) and executive control (Ma et al., 2015; Skoblenick and Everling, 2012, 2014) in saccade tasks. However, these studies have not specifically evaluated how reduced NMDAR function changes spike timing dynamics in prefrontal ensembles. This may be a crucial level of analysis because changes in spike timing could influence synaptic connectivity of prefrontal circuits via spike-timing-dependent synaptic plasticity mechanisms (Feldman, 2012) and also provide a proxy metric tracking the functional disconnection of prefrontal circuits (Friston, 1999, 2002; Stephan et al., 2009) (Figures 5B and 5D).

We report the following primary findings. First, the timing with which pairs of prefrontal neurons generated action potentials relative to one another was dominated by joint spike events that occurred at “0-lag,” meaning that two neurons fired an action potential nearly simultaneously, within ±1 ms, more often than predicted by chance under the assumption that neurons fire independently (Figures 2 and 4). Second, the pairwise 0-lag spike correlation was strongly modulated during behavior, peaking around the time of the motor response and continuing into the inter-trial interval when trial feedback (reward) was delivered (Figure 4). Third, the pattern of functional coupling between neurons was significantly correlated with the different task-related patterns of activity of the neurons (Figure 7), establishing a link between functional coupling detected by correlation analyses and the functional properties of prefrontal neurons. Fourth, blocking NMDARs acutely reduced 0-lag functional coupling in prefrontal cortex (Figures 2 and 4). Fifth, periodically blocking NMDARs functionally decoupled prefrontal circuits as indicated by a persistent

reduction both in the prevalence and strength of 0-lag CCH (Figure 2) and lagged TE (Figure 5) causal interactions between neurons in the saline condition relative to the drug-naive condition.

Activity-Dependent Disconnection in Schizophrenia

These observations lead us to consider whether spike-timing-dependent synaptic disconnection might be a primary pathogenic driver in schizophrenia, disconnecting prefrontal circuits via an activity-dependent mechanism (Figure 8). In this theory, genetic mutations that (1) are likely to disrupt NMDAR synaptic function (Fromer et al., 2014; Krystal et al., 2002; MacDonald and Chafee, 2006; Schizophrenia Working Group of the Psychiatric Genomics Consortium, 2014), and (2) could lead to excessive synaptic pruning in adolescence (Sekar et al., 2016), produce a pathophysiological condition in prefrontal networks wherein the fidelity of synchronous spiking in connected neurons falls below a critical threshold. That loss of synchronous or near-synchronous spiking, operating through spike-timing-dependent synaptic plasticity mechanisms (Feldman, 2012), would then lead to additional synaptic disconnection of prefrontal networks through an activity-dependent process. The net result would be that Hebbian plasticity, operating effectively in reverse to synaptically disconnect neurons that do not exhibit synchronous spiking, drives prefrontal networks into a state of progressively reduced synaptic connectivity that ultimately produces the clinical symptoms and cognitive deficits of the disease. Because a spike timing defect would be likely to make a connectivity deficit worse, and vice versa, spike timing disruption and functional disconnection could accelerate each other as they progressed in parallel during disease pathogenesis. This positive feedback between a progressive spike timing defect and progressive functional disconnection of prefrontal networks could create a persistently disconnected state that, once entered into, could be difficult to get out of. We found, in support of this theory, that 0-lag spike correlation seen in the saline condition progressively declined as a function of the number of preceding days of phencyclidine injection (Figure S4), and the reduction in synchronous spiking was associated with the persistent functional disconnection of prefrontal circuits (Figures 2, 4, and 5). These findings may suggest that in schizophrenia, insults that impair NMDAR-mediated synaptic transmission could first reduce synchronous spiking in prefrontal networks, which then start to synaptically disconnect via a spike-timing-dependent mechanism.

We administered an NMDAR antagonist systemically in this study. Two advantages of this strategy are that systemic administration produces strong behavioral effects (inducing an error pattern in monkeys similar to that seen in patients with schizophrenia; Figure 1G), as well as a global modulation of NMDAR function that may mimic the effects of schizophrenia risk mutations likely to modify NMDAR synaptic communication broadly throughout the brain (Fromer et al., 2014; Krystal et al., 2002; MacDonald and Chafee, 2006; Schizophrenia Working Group of the Psychiatric Genomics Consortium, 2014). Because we employed systemic administration, NMDAR synaptic function was reduced broadly throughout the brain and changes in the timing of spikes in prefrontal neurons may have been driven by a change in the temporal structure of prefrontal inputs.

Although we have observed a change in spike timing and a change in functional connectivity in prefrontal cortex, our data do not address whether a change in spike timing causes functional disconnection. It will be important to evaluate whether changes in spike synchrony and functional coupling are common to multiple risk factors for schizophrenia (such as risk mutations), to evaluate whether a perturbation in spike timing is a common endpoint of the multiple causal factors and pathogenic trajectories that lead to the disease. Finally, NMDARs play a direct role in mediating spike-timing-dependent synaptic plasticity themselves, and loss of this synaptic mechanism, apart from changes in spike timing, could contribute to the functional disconnection we have observed. As spike timing plays a role in controlling the sign of the change in synaptic strength mediated by NMDAR, whether long term potentiation or depression (Feldman, 2012), the timing of action potentials could be a key pathogenic variable in controlling the net impact of NMDAR insult on cortical connectivity.

Prior Observations of Reduced Spike and Network Synchrony in Animal Models

Prior recording studies have shown that 0-lag synchronous spiking is a prominent feature of spike timing dynamics in monkey prefrontal cortex (Constantinidis et al., 2001; Pipa and Munk, 2011), that the frequency of joint spike events is modulated during behavior independently of firing rate (Pipa and Munk, 2011; Riehle et al., 1997), and that the strength of 0-lag interactions scales with the similarity in spatial tuning properties of prefrontal neurons (Constantinidis et al., 2001). Artificial neural network models have shown that reciprocal excitatory circuits can self-organize to generate 0-lag spike synchrony in spite of long conduction delays (Vicente et al., 2008). In addition, 0-lag spiking between prefrontal neurons is found within rat medial prefrontal cortex and blocking NMDARs reduces the strength of this 0-lag synchrony while also reducing the Fano factor (Molina et al., 2014), paralleling our observations in monkey prefrontal cortex (Figures 2 and 3). Deletion of NMDARs on parvalbumin interneurons reduces task-evoked gamma oscillations (Carlen et al., 2012), and reduction in oscillatory synchrony at the network level could contribute to the reduction in synchrony we observed at the spiking level to result from pharmacological blockade of NMDAR (Figures 2, 4, and 5) and in prior studies (Molina et al., 2014). Sigurdsson et al. (2010), investigating prefrontal-hippocampal synchrony in the 22q11.2 microdeletion mouse genetic model of schizophrenia, found reduced spike-field phase locking in the theta band and reduced gamma band phase coherence between PFC and hippocampus in mutants. This suggests that genetic risk for schizophrenia reduces the consistency with which spike timing is phase-locked to network oscillations, and this could contribute further to the reduced spike synchrony we observed.

Interestingly, a recent study in primates revealed that synchrony between the prefrontal cortex and hippocampus is strongly modulated during behavior in executive control tasks peaking around the time of the motor response and trial feedback (Brincat and Miller, 2015), which is similar to the time at which we found 0-lag spike synchrony between prefrontal neurons to peak during DPX performance (Figures 4A and 4H). Skoblenick et al. (2016) investigated prefrontal synchrony in a rule-based saccade task, finding an increase in LFP beta power around the time of trial feedback following the saccade on correct trials that depended on NMDAR synaptic mechanisms. These prior observations suggest that there is a

period of NMDAR-dependent prefrontal network synchrony that occurs around the time of the response and trial feedback. That oscillatory network dynamic could contribute to the 0-lag spike synchrony we observed at the neural level in the present study.

Relation of Spike-Timing-Dependent Synaptic Disconnection to Prior Theories

The idea that schizophrenia results from a disconnection of cortical networks, attributed to Carl Wernicke (Friston, 2002; Stephan et al., 2009), has a long history. But neurophysiological evidence of impaired temporal coordination of neural activity in the brains of patients has more recently given the theory a neurophysiological basis (Friston, 1999; Friston and Frith, 1995; Lawrie et al., 2002; Scariati et al., 2016; Stephan et al., 2009). Consistent with this hypothesis, functional imaging studies in patients have repeatedly shown that schizophrenia weakens functional coupling in prefrontal networks based on reduced temporal correlations in BOLD signal across brain areas (Kang et al., 2011; Kubota et al., 2013; Lawrie et al., 2002; Mitelman et al., 2005; Mukherjee et al., 2016; Scariati et al., 2016; Tu et al., 2012, 2013). Measurements of brain activity at higher temporal resolution using electroencephalograms (EEG) and magnetoencephalography (MEG) have shown reduced synchrony in gamma band during task performance (Dale et al., 2016; Uhlhaas and Singer, 2015). The spike-timing-dependent synaptic disconnection theory is an elaboration of these prior theories extending the synchrony deficits described at larger physical scales within the brain to the level of spiking neurons, considering the impact of spike timing disruption on synaptic connectivity operating through spike-timing-dependent plasticity mechanisms. Our data support the theory that activity-dependent retraction of dendritic spines (Lai and Ip, 2013), driven in part by a reduction in synchronous and near-synchronous spiking in prefrontal networks (Figures 2, 4, and 5), could contribute to the reduced density of dendritic spines on pyramidal cells that has been repeatedly observed in postmortem analysis of the brains of patients, particularly in prefrontal cortex (Glantz and Lewis, 2000; Kolluri et al., 2005; MacDonald et al., 2017; Shelton et al., 2015).

Conclusion

We observed an association between a reduction in spike timing synchrony in prefrontal circuits and persistent functional disconnection of prefrontal circuits downstream of pharmacological blockade of NMDAR-mediated synaptic transmission. Multiple lines of evidence link NMDAR dysfunction to schizophrenia, suggesting that the cellular-level asynchrony and disconnection seen here may also occur in patients. We propose an activity-dependent disconnection theory of schizophrenia in which a perturbation in NMDAR synaptic transmission, in combination with other causal factors in the disease, leads to the loss of spike synchrony that drives synaptic disconnection of prefrontal circuits over time via a spike-timing-dependent process.

STAR★METHODS

CONTACT FOR REAGENT AND RESOURCE SHARING

Further information and requests for resources should be directed to and will be fulfilled by the Lead Contact, Matthew V. Chafee (chafe001@umn.edu)

EXPERIMENTAL MODEL AND SUBJECT DETAILS

Monkeys

Two adult male rhesus macaques (8-10 kg) were used for neural recording in prefrontal cortex during DPX task performance in this study. Both animals had participated in a prior study in which they received subanesthetic doses of ketamine to evaluate the impact of NMDAR blockade on DPX task performance (Blackman et al., 2013). Basic features of task-related signals in prefrontal cortex were described in a prior report (Blackman et al., 2016). Additional experimental details can be found there. All animal care and experimental procedures conformed to National Institutes of Health guidelines and complied with protocols approved by the Animal Care and Use Committee at the University of Minnesota and Minneapolis Veterans Administration Medical Center.

METHOD DETAILS

Surgery

Monkeys were prepared for acute neural recording in an aseptic surgery performed under general gas (isoflurance, 1%–2%) anesthesia. Craniotomies were made overlying the dorsolateral prefrontal and posterior parietal cortex. Spiking dynamics based on analysis of neural activity in prefrontal cortex are reported here. Plastic recording chambers were cemented over the craniotomies using surgical bone cement anchoring the chambers to screws placed in the surrounding surface of the skull to enable neural recording. Titanium posts were attached to the skull to make it possible to stabilize head position for neural recording. Monkeys received injectable analgesics for several days postoperatively (Buprenex; 0.05 mg/kg twice a day, i.m.).

Behavioral task

We characterized prefrontal spiking dynamics during the performance of a dot-pattern expectancy (DPX) version of the AX continuous performance task (AX-CPT). The dot-pattern variant of this task replaces letters with dot patterns. One cue dot pattern was designated the A-cue, whereas several alternative dot patterns were collectively designated B-cues (Figure 1C). Likewise, one probe dot pattern was designated the X-probe, whereas several alternative dot patterns were collectively designated Y-probes (Figure 1D). In each trial, a cue was followed by a probe stimulus. If the cue-probe sequence was A followed by X, the trial was considered a target trial and the target response was required (the correct response on target trials was for the monkey to move a joystick to the left with his right hand) (Figure 1A). All other cue-probe sequences were nontarget trials requiring nontarget responses (the monkey moved the joystick to the right with his right hand) (Figure 1B). Monkeys initiated the trial by directing their gaze toward a central fixation stimulus (cross) presented on a video monitor. They were required to maintain their gaze fixated on the stimulus within a 3.3° window for the duration of the trial. After 0.5 s of central gaze fixation, a cue stimulus was presented centered on the fixation target, for a period of 1.0 s, and then disappeared (Figures 1A and 1B). A 1.0 s delay period followed the cue period, at the end of which a probe stimulus was presented centered on the fixation target for 0.5 s, and then disappeared. Stimulus timing was fixed, as in human studies (Jones et al., 2010). An

inter-trial interval of 1.36 s followed the offset of the probe stimulus. At the end of the inter-trial interval, the fixation cross reappeared indicating the beginning of the next trial. Monkeys could respond any time after probe onset up through the first 1.0 s of the inter-trial interval. If they moved the joystick in this interval in the correct direction based on the cue-probe sequence they were rewarded with 0.1 mL drop of juice.

Combinations of cues and probes defined four different trial types (AX, AY, BX and BY). We presented these four trial types in the following proportion. Most trials (69%) were AX (target trials), to increase the prepotency of the target response and establish a habit to produce the target response when the X-probe appears. The remaining 31% of trials were nontarget trials and were either AY (12.5%), BX (12.5%), or BY (6%). This is the same proportion of trial types used to characterize cognitive deficits in patients with schizophrenia (Jones et al., 2010). Most trial sets included between 200 and 400 correctly performed trials. We restrict the analysis of neural dynamics in the present report (other than analyses contributing to Figure S6) to correctly performed DPX trials. In addition, we recorded neural activity on balanced trial sets made up of 20 trials each of the four trial types (AX, AY, BX and BY). The cue (A versus B) and probe (X versus Y) stimuli were uncorrelated in the balanced trial sets and neural data recorded during balanced sets was used to assign neurons to functional classes based on an ANCOVA (below).

Experimental conditions

In the Drug condition, we recorded prefrontal neural activity for a period of several hours following an intramuscular injection of an NMDAR antagonist (Phencyclidine, Sigma Pharmaceuticals diluted in sterile saline at 5 mg / ml). We administered the drug at a dose of 0.25-0.30 mg/kg (with the exception of an injection of 0.20 mg/kg in monkey M1 at the start of these experiments). In the Saline condition, we recorded prefrontal neural activity for a period of several hours following an intramuscular injection of an equivalent volume of sterile saline (0.05 – 0.06 ml/kg, or a total volume of approximately 0.5 ml). Injections were administered in the quadriceps muscle. We opted to hold the dose of phencyclidine constant across days because this dose produced a reliable cognitive deficit (Figure 1G), and this maximized the size of the neural sample in the Drug condition (and hence statistical power to detect differences between conditions) without having to divide neurons in the Drug condition by dose. In the drug-Naive condition, neural data were recorded before animals had received their first injection of phencyclidine. (On some days of drug-Naive data collection, animals received no injection, on other days, they received an injection of sterile saline prior to recording.) After neural data had been recorded in the drug-Naive condition, interleaved daily injections of PCP (Drug condition) or saline (Saline condition) began. Phencyclidine is an anesthetic, and at the subanesthetic doses we employed, monkeys were drowsy for a period and then began to work consistently on the DPX task. Data included in the Drug condition consisted of neural activity recorded following an injection of phencyclidine. Data included in the Saline condition consisted of neural activity recorded following an injection of saline, with the additional constraint that monkeys had received phencyclidine on a prior day (e.g., after first exposure to phencyclidine). (See Figure S1 for the daily sequence of experimental conditions administered to each animal.)

Neural recording

We recorded the spiking activity of small neural ensembles of individually isolated prefrontal neurons using an Eckhorn microelectrode drive (Thomas recording, GmbH) that advanced 16 thin (70 μm o.d.) glass coated platinum iridium microelectrodes independently into the brain under computer control. We adjusted the depths of the electrodes to maximize the numbers of action potential waveforms from spiking neurons that were detectible above the background. We isolated the waveforms of individual neurons online using spike sorting software (Alpha Omega Engineering; Nazareth, Israel). Spike times were stored with 40 μs resolution (DAP 5200a Data Acquisition Processor; Microstar Laboratories, Belleview, WA).

We recorded the activity of 89 neural ensembles containing on average 19 individually isolated neurons for a total of 1708 prefrontal neurons. The neural data were divided between the three experimental conditions as follows: drug-Naive (38 ensembles, 753 neurons), Saline (16 ensembles, 288 neurons), and Drug (35 ensembles, 667 neurons). (The number of prefrontal ensembles analyzed in this report does not identically match the injection schedule in Figure S1 because on some days neural recordings were not conducted in prefrontal cortex or the monkey did not perform the full task).

QUANTIFICATION AND STATISTICAL ANALYSIS

Artifact removal

We detected a small overrepresentation of action potentials at fixed times relative to the motor response that were most likely caused by electrical artifact. These excess spikes were manually removed through visual inspection of the data based on their consistent relationship to the time of the motor response, and both the CCH and TE correlation analyses were applied to the filtered data after these spurious spikes were removed. We confirmed that the presence of the 0-lag peak in the CCH and its reduction in the Drug relative to drug-Naive and Saline conditions (Figure 2) persisted in a separate CCH analysis using spike trains restricted to a window beginning at probe onset and extending to 25 ms before the motor response that excluded the times when spurious spikes occurred (Figure S8).

Cross-correlation analyses

To quantify the frequency distribution of spike pairs in simultaneously recorded neurons as a function of the lag (1 ms resolution) between the two spikes, we computed cross-correlation histograms (CCHs) (Perkel et al., 1967). Correlations in spike times in two neurons can be expected to occur by chance at a level that scales with the firing rates of the two neurons (Baker and Lemon, 2000). To account for this, we applied the following rate normalization procedure. For each neuron pair, we generated 100 bootstrap CCHs by shifting each spike by a random interval between −30 and +30 ms and then computed a CCH using the jittered spike times. (Reducing the range of time over which spikes were jittered to ± 10 ms did not influence which neuronal pairs had significant 0-lag CCH peaks, so that the size of the jitter window did not alter the pattern of coupling.) We considered the mean count of joint spikes in each bin across the 100 bootstrap CCHs constructed for that neuron pair to be the

expected baseline count of joint spikes under the null hypothesis that the spike trains of the two neurons were independent, and joint spiking was driven by modulations in firing rate alone. For each neuron pair, we computed the sum of joint spike counts in the −1,0 and +1 lag bins (defining this as the 0-lag peak height) in the original CCH and in each of the 100 spike-time jittered CCHs. We identified neuron pairs as significantly coupled at 0-lag if the 0-lag CCH peak height in the original data exceeded the 99th percentile of the bootstrap distribution of 0-lag peak heights computed using spike-time jittered data. We used this method of jittering spike times rather than shift predictors or trial shuffling because it applied randomness to the precise timing of action potentials but preserved local modulations in firing rate as well as the relationship between spike trains and behavioral variables such as the stimuli presented and response at the trial level. Data from cue onset to the end of the trial were included in this analysis, and only CCHs containing > 100 spike pairs were analyzed. Neuron pairs in which the two neurons were recorded on the same electrode were not included in this analysis to eliminate correlations that could be the result of inaccurate spike sorting. To construct the population-average CCHs (Figure 2C), for each neuron pair we first normalized the CCH by dividing joint spike counts in each bin by the mean count in the same bin calculated over the bootstrap distribution. We then averaged the normalized CCHs over all neuron pairs. To compute the median 0-lag CCH peak height in each experimental condition (Figure 2D), we first normalized the 0-lag peak in each neuron pair by dividing it by the mean 0-lag peak averaged over the 100 spike-jittered CCHs (from the same neuron pair). We then computed the median of the normalized peaks over all neuron pairs recorded in each experimental condition (along with the 95% bootstrap confidence interval of the median; 1000 iterations)

We characterized the variability of spike counts by calculating the Fano Factor in each neuron. All spike trains were divided into time bins of 50 ms, and the Fano Factor was computed as the ratio of the variance to the mean of the spike counts across all bins for each neuron.

Trial time resolved cross-correlation analysis

To analyze how pairwise spike synchrony is modulated during task performance we used an approach inspired by previous work (Aertsen et al., 1989; Gerstein and Perkel, 1969; Grün et al., 2002). The time interval of interest is subdivided into small bins of width Δt. Activity of neuron i in a given trial is represented by a binary variable $s_i(t)$ that can take on two values: 1 if in the time bin t one or more spikes are present (referred to as ‘a spike’ in the rest of our consideration), and 0 if there are no spikes. Correspondingly, time-lagged joint spike activity of neurons i and j is described by the product $s_i(t)s_j(t+\tau)$: it is 1 if neuron i fired a spike in the time bin t and neuron j fired a spike in the time bin $t+\tau$; otherwise it is 0. We assume that spike firing statistics of neurons do not change across repeated K trials of the same task, so that at any instant of time low order moments of the underlying binary variables can be reliably estimated by averaging over trials. In this framework, the mean spike rate of neuron i in the time bin t is given by $p_i(t) = \langle s_i(t) \rangle$, and its variance by $\sigma_i^2(t) = \langle s_i^2(t) \rangle - \langle s_i(t)^2 \rangle = p_i(t)(1 - p_i(t))$, where $\langle \bullet \rangle$ denotes the trial averaging operation. Correspondingly, the mean time-lagged joint spike rate is given as $p_{ij}(t, t+\tau) = \langle s_i(t)s_j(t+\tau) \rangle$. Note that if activities of neurons i and j are independent, then $\langle s_i(t)s_j(t+\tau) \rangle = \langle s_i(t) \rangle \langle S_j(t$

$+\ \tau)\rangle$ and, thus, $p_{ij}(t,\ t+\ \tau) = p_i(t)p_j(t+\ \tau)$. Delayed spike synchrony between neurons i and j, as their respective spikes occur in the time bins t and $t+\ \tau$, can be characterized in terms of the deviation of the frequency of such events from the expected frequency when neurons fire spikes with the same rates $p_i(t)$ and $p_j(t+\ \tau)$ but independently: $p_{ij}(t,\ t+\ \tau) - p_i(t)p_j(t+\ \tau)$. We divide this expression, which is analogous to the cross-covariance function, by the standard deviation of the expected frequency of spike synchrony for independently firing neurons, $\sigma_i(t)\sigma_j(t+\ \tau)$, to obtain a normalized (Pearson) correlation measure $\rho_{ij}(t,\ t+\ \tau)$ that varies between −1 (fully anti-correlated) to 0 (fully uncorrelated) to +1(fully correlated): $\rho_{ij}(t,t+\ \tau) = (p_{ij}(t,t+\ \tau) - p_i(t)p_j(t+\ \tau))/\sigma_i(t)\sigma_j(t+\ \tau)$.

In our consideration, the parameter Δt defines the spike timing resolution. To assess the precision of spike synchrony in PFC circuits it is required to keep its value sufficiently small. On the other hand, the firing rates of PFC neurons are relatively low, on the order of 10 Hz and, for example, in a time bin of the duration $\Delta t = 1$ ms we expect to observe a spike in only one out of $K = 100$ trials. Therefore, to increase the number of counts and improve the estimates of single and joint neuron spike statistic while keeping Δt sufficiently small (and thus spike timing resolution sufficiently high), we combined data within non-overlapping time windows of width $\Delta T = M{\cdot}\Delta t$ by pooling together observations in M consecutive Δt-bins over K trials. This allowed to carry out the averaging operation over a larger number of effective 'trials', in essence increasing them form K to $K{\cdot}M$. Thus, by reducing the temporal resolution of spike synchrony analysis (defined by the parameter ΔT) one might be able to keep a relatively high spike timing resolution (defined by the parameter Δt) providing reliable estimates of spike rates. Results in Figure 4 are shown for $\Delta t = 1$ ms and $\Delta T = 50$ ms (i.e., $M = 50$). Since in most of recordings there were at least $K = 140$ correctly performed trials this choice of parameters provided for each pair of neurons at each 50 ms temporal window a large number of effective trials $K{\cdot}M = 140{\cdot}50 = 7{,}000$ (i.e., observations) and, thus, allowing for a high 1 ms spike timing resolution. Also, since the size of bin Δt was so small, no more than one spike occurred in a bin.

Transfer entropy

Transfer entropy was calculated between neuron pairs using the algorithm of (Ito et al., 2011). We employed their open source MATLAB transfer entropy toolbox – the details of their algorithm, along with a software package and sample dataset for MATLAB, are included on the lab's project website (https://code.google.com/archive/p/transfer-entropy-toolbox/). We computed higher-order transfer entropy from neuron J to neuron I as defined by Ito and colleagues as:

$$TE_{J\to I} = \sum p\left(i_{t+1}, i_t^{(k)}, j_{t+1-d}^{(l)}\right) log_2 \frac{p\left(i_{t+1} \middle| i_t^{(k)}, j_{t+1-d}^{(l)}\right)}{p\left(i_{t+1} \middle| i_t^{(k)}\right)}$$

The activity states i and j of neurons I and J, respectively, are represented as 1 if the neuron produces a spike in the time bin t or as 0 otherwise. The order parameters k and l represent the number of time bins in the past describing the spiking patterns of neurons I and J, respectively when predicting the activity state of neuron I. The delay parameter d represents

the lag at which to consider the influence of neuron *J* on neuron *I*. We used 1 ms time bins to evaluate transfer entropy, and adopted input parameters $k = 1$, $I = 1$, and maximum delay (lag) = 10 ms. (Lags in Figure 5 are extended to 30 ms for illustration purposes.)

Transfer entropy measures the amount of information about the activity state of the target neuron *I* available from an activity history of the transmitting neuron *J*, d-time bins earlier, that is in addition to the information provided by the history of spiking activity of the target neuron *I* alone. Transfer entropy is nonnegative and it is zero if there is no causal influence from *J* to *I*.

Pairwise relationships were evaluated using TE analysis of spike trains starting at cue onset and extending through the end of the DPX trial. In general, naive estimation of information-theoretic quantities from limited experimental samples results in positive bias (Panzeri et al., 2007). Therefore, all TE estimates were bias-corrected using bootstrap distributions in which potential causal interactions were destroyed. Specifically, for each neuron pair, we constructed 1000 bootstrap samples and estimated TE functions after shifting each spike by a random interval between −30 and 30 ms (an analysis using ± 10 ms shifts yielded nearly identical results). Bias-corrected TE values were obtained by subtracting the mean of the bootstrap values from the original, at each time bin. (Nearly identical results were obtained when TE values were biased corrected by subtracting the median of the bootstrap distribution.)

To assess the statistical significance of lagged interactions between neurons using TE, we first identified the maximum TE value (‘peak’) for each neuron pair in the range of 1 to 10 ms lags. We compared this peak TE value to the bootstrap distribution of peak TE values obtained after jittering spike times. This bootstrap distribution was generated by finding the peak TE value of each bootstrap sample in the same 1-10 ms lag window, regardless of the lag bin in which the peak was found. We considered the neuronal pair significantly coupled if the peak of the original TE time course exceeded the 99.9^{th} percentile of the bootstrap distribution of TE peaks across all bins.

Relation between neural signaling and functional coupling

To evaluate whether the pattern of functional coupling between neurons based on an analysis of their spike timing reflected the functional properties of the neurons (based on their behaviorally defined signals), we performed the following analysis. We described each neuron pair by two dichotomous variables indicating: (1) whether the pair contained two neurons with the same task-defined pattern of activity (defined below), and (2) whether the pair was functionally coupled (by CCH or TE analysis). We then performed a test of association to determine whether the two dichotomous variables were statistically related across neuron pairs (whether knowing something about function provided information about connectivity). To that end, we sorted each neuron into one of two classes, depending on their activity during the task (Figures 7A and 7B). Neurons in class I are Groups 2, 3 and 4 from (Blackman et al., 2016) combined. Neurons in class II included neurons from Groups 5 and 6 (Blackman et al., 2016).

Neuron groups illustrated in Figure 5 of Blackman et al. (2016) were defined on the basis of the trial epochs in which neurons exhibited significant modulation in firing rate as a function of the cue (A or B), probe (X or Y) or response (target or nontarget) by ANCOVA, in combination with the stimulus or response preference of the neurons. This captured strong biases at the population level to encode different stimuli at different times in the trial, with single neurons often switching their cue preference between the cue and probe periods.

Class I consisted of neuron groups 2, 3 and 4. Group 2 neurons were identified as having significantly elevated activity on A-cue (relative to B-cue) trials during the delay or probe periods. During the cue period, the same neurons tended to exhibit elevated activity on B-cue trials. Therefore, the cue preference of Group 2 neurons switched from B-cues early to A-cues late in the trial. Group 3 neurons were identified as having significant B-cue preference during the delay period. The same neurons tended to exhibit B-cue preference during the cue period and AY preference during the probe period as well. Therefore Group 3 neurons also generally exhibited a switch in preference for B-cues early to A-cues late in the trial. Group 4 neurons were identified as having significant B-cue preference in the cue period, or Y-probe preference during the probe period. These neurons exhibited greatest activity on AY trials. Therefore neurons in Groups 2-4 generally preferred the B-cue during the cue period, and the A-cue during the probe period, with particularly strong probe period activation on AY trials (Blackman et al., 2016).

Class II consisted of neuron groups 5 and 6. Group 5 neurons were defined as those which exhibited significantly greater activity during the probe period on B-cue than A-cue trials, or as those which exhibited significantly greater activity during the response period on nontarget than target response trials. Group 6 neurons were defined as those which exhibited significantly greater activity during the probe period on X-probe than Y-probe trials. Based on the aggregation of these functional groups into the broader class I and II classification, we evaluated the relationship between functional coupling and task-related activity.

We restricted the analysis to neuron pairs in which both neurons were assigned either to class I or class II, and defined ‘like pairs’ as neuron pairs in which the two neurons belonged to the same physiological class (either both neurons belonged to class I or to class II), and ‘unlike pairs’ as neuron pairs in which one neuron belonged to class I and the other to class II. We then applied Fisher’s exact test to test whether the proportion of significantly coupled neurons differed between like and unlike pairs, considering coupling both at 0-lag (based on the CCH analysis) and nonzero lag (based on the TE analysis). Differences in coupling probability between like and unlike pairs quantified a relationship between functional coupling and physiological class, which we term the coupling bias.

We then addressed whether the coupling bias was significantly influenced by experimental condition (Figure S7) as follows. We defined the condition effect on coupling as the difference in coupling bias between all pairs of experimental conditions (naive versus drug, naive versus saline, saline versus drug). We then evaluated whether the condition effect on coupling bias was significant in a permutation test. We considered the condition effect computed from the original data to be significant if the difference in coupling biases between experimental conditions exceeded the 95^{th} percentile of a bootstrap distribution of

differences in coupling biases between conditions computed after shuffling the relationship between neuron pairs and experimental condition (1000 iterations).

DATA AND SOFTWARE AVAILABILITY

Data and MATLAB analysis scripts are available upon request from M. Chafee (chafe001@umn.edu).

Supplementary Material

Refer to Web version on PubMed Central for supplementary material.

ACKNOWLEDGMENTS

We thank Dean Evans for lab and project management as well as his assistance with surgeries, animal care, and neural recordings; Dale Boeff for his assistance with neurophysiological recording system design and construction, as well as computer programming for signal processing and data analysis; Sofia Sakellaridi for her assistance with neural recordings; and Aisha Mohamed for her assistance with preliminary data analysis. Support for this work was provided by the National Institute of Mental Health (R01MH077779 and R01MH107491 to M.V.C., 5F30MH108205-02 to J.L.Z., R25 MH101076 to R.K.B., and F31MH109238 to A.L.D.), the National Institute of General Medical Sciences (T32 GM008244 to R.K.B. and T32GM847121 to A.L.D.), Wilfred Wetzel Graduate Fellowship (to R.K.B.), Minnesota Medical Foundation (to M.V.C. and T.I.N.), Winston and Maxine Wallin Neuroscience Discovery Fund (to M.V.C.), MnDrive Neuromodulation Fellowship (to A.L.D.), American Brain Sciences Chair, and the Department of Veterans Affairs (to B.A.). This material is the result of work supported with resources and the use of facilities at the Minneapolis VA Health Care System. The contents do not represent the views of the U.S. Department of Veterans Affairs or the United States Government.

REFERENCES

Aertsen AM , Gerstein GL , Habib MK , and Palm G (1989). Dynamics of neuronal firing correlation: modulation of “effective connectivity”. J. Neurophysiol 61, 900–917.2723733

Amit DJ , and Brunel N (1997). Model of global spontaneous activity and local structured activity during delay periods in the cerebral cortex. Cereb. Cortex 7, 237–252.9143444

Averbeck BB , and Chafee MV (2016). Using model systems to understand errant plasticity mechanisms in psychiatric disorders. Nat. Neurosci 19, 1418–1425.27786180

Baker SN , and Lemon RN (2000). Precise spatiotemporal repeating patterns in monkey primary and supplementary motor areas occur at chance levels. J. Neurophysiol 84, 1770–1780.11024069

Barch DM , and Ceaser A (2012). Cognition in schizophrenia: core psychological and neural mechanisms. Trends Cogn. Sci 16, 27–34.22169777

Barch DM , Carter CS , MacDonald AW , Braver TS , and Cohen JD (2003). Context-processing deficits in schizophrenia: diagnostic specificity, 4-week course, and relationships to clinical symptoms. J. Abnorm. Psychol 112, 132–143.12653421

Blackman RK , Macdonald AW , and Chafee MV (2013). Effects of ketamine on context-processing performance in monkeys: a new animal model of cognitive deficits in schizophrenia. Neuropsychopharmacology 38, 2090–2100.23660706

Blackman RK , Crowe DA , DeNicola AL , Sakellaridi S , MacDonald AW , and Chafee MV (2016). Monkey prefrontal neurons reflect logical operations for cognitive control in a variant of the AX continuous performance task (AX-CPT). J. Neurosci 36, 4067–4079.27053213

Brincat SL , and Miller EK (2015). Frequency-specific hippocampal-prefrontal interactions during associative learning. Nat. Neurosci 18, 576–581.25706471

Camchong J , MacDonald AW , Bell C , Mueller BA , and Lim KO (2011). Altered functional and anatomical connectivity in schizophrenia. Schizophr. Bull 37, 640–650.19920062

Carlen M , Meletis K , Siegle JH , Cardin JA , Futai K , Vierling-Claassen D , Ruhlmann C , Jones SR , Deisseroth K , Sheng M , et al. (2012).A critical role for NMDA receptors in parvalbumin interneurons for gamma rhythm induction and behavior. Mol. Psychiatry 17, 537–548.21468034

Carter CS , Minzenberg M , West R , and Macdonald A (2012). CNTRICS imaging biomarker selections: executive control paradigms. Schizophr. Bull 38, 34–42.22114099

Constantinidis C , Franowicz MN , and Goldman-Rakic PS (2001). Coding specificity in cortical microcircuits: a multiple-electrode analysis of primate prefrontal cortex. J. Neurosci 21, 3646–3655.11331394

Dale CL , Brown EG , Fisher M , Herman AB , Dowling AF , Hinkley LB , Subramaniam K , Nagarajan SS , and Vinogradov S (2016). Auditory cortical plasticity drives training-induced cognitive changes in schizophrenia. Schizophr. Bull 42, 220–228.26152668

Dias EC , McGinnis T , Smiley JF , Foxe JJ , Schroeder CE , and Javitt DC (2006). Changing plans: neural correlates of executive control in monkey and human frontal cortex. Exp. Brain Res 174, 279–291.16636795

Feldman DE (2012). The spike-timing dependence of plasticity. Neuron 75, 556–571.22920249

Friston KJ (1999). Schizophrenia and the disconnection hypothesis. Acta Psychiatr. Scand. Suppl 395, 68–79.10225335

Friston KJ (2002). Dysfunctional connectivity in schizophrenia. World Psychiatry 1, 66–71.16946855

Friston KJ , and Frith CD (1995). Schizophrenia: a disconnection syndrome? Clin. Neurosci 3, 89–97.7583624

Fromer M , Pocklington AJ , Kavanagh DH , Williams HJ , Dwyer S , Gormley P , Georgieva L , Rees E , Palta P , Ruderfer DM , et al. (2014). De novo mutations in schizophrenia implicate synaptic networks. Nature 506, 179–184.24463507

Garofalo M , Nieus T , Massobrio P , and Martinoia S (2009). Evaluation of the performance of information theory-based methods and cross-correlation to estimate the functional connectivity in cortical networks. PLoS One 4, e6482.19652720

Gerstein GL , and Perkel DH (1969). Simultaneously recorded trains of action potentials: analysis and functional interpretation. Science 164, 828–830.5767782

Glantz LA , and Lewis DA (2000). Decreased dendritic spine density on prefrontal cortical pyramidal neurons in schizophrenia. Arch. Gen. Psychiatry 57, 65–73.10632234

Goldman-Rakic PS (1999). The physiological approach: functional architecture of working memory and disordered cognition in schizophrenia. Biol. Psychiatry 46, 650–661.10472417

Grün S , Diesmann M , and Aertsen A (2002). Unitary events in multiple single-neuron spiking activity: II. Nonstationary data. Neural Comput. 14, 81–119.11747535

Insel TR (2010). Rethinking schizophrenia. Nature 468, 187–193.21068826

Ito S , Hansen ME , Heiland R , Lumsdaine A , Litke AM , and Beggs JM (2011). Extending transfer entropy improves identification of effective connectivity in a spiking cortical network model. PLoS One 6, e27431.22102894

Jones JA , Sponheim SR , and MacDonald AW (2010). The dot pattern expectancy task: reliability and replication of deficits in schizophrenia. Psychol. Assess 22, 131–141.20230159

Kang SS , Sponheim SR , Chafee MV , and MacDonald AW (2011). Disrupted functional connectivity for controlled visual processing as a basis for impaired spatial working memory in schizophrenia. Neuropsychologia 49, 2836–2847.21703287

Kirov G , Pocklington AJ , Holmans P , Ivanov D , Ikeda M , Ruderfer D , Moran J , Chambert K , Toncheva D , Georgieva L , et al. (2012). De novo CNV analysis implicates specific abnormalities of postsynaptic signalling complexes in the pathogenesis of schizophrenia. Mol. Psychiatry 17, 142–153.22083728

Kolluri N , Sun Z , Sampson AR , and Lewis DA (2005). Lamina-specific reductions in dendritic spine density in the prefrontal cortex of subjects with schizophrenia. Am. J. Psychiatry 162, 1200–1202.15930070

Korndörfer C , Ullner E , García-Ojalvo J , and Pipa G (2017). Cortical spike synchrony as a measure of input familiarity. Neural Comput. 29, 2491–2510.28599117

Krystal JH , Anand A , and Moghaddam B (2002). Effects of NMDA receptor antagonists: implications for the pathophysiology of schizophrenia. Arch. Gen. Psychiatry 59, 663–664.12090822

Kubota M , Miyata J , Sasamoto A , Sugihara G , Yoshida H , Kawada R , Fujimoto S , Tanaka Y , Sawamoto N , Fukuyama H , et al. (2013). Thalamocortical disconnection in the orbitofrontal region associated with cortical thinning in schizophrenia. JAMA Psychiatry 70, 12–21.22945538

Lai KO , and Ip NY (2013). Structural plasticity of dendritic spines: the underlying mechanisms and its dysregulation in brain disorders. Biochim. Biophys. Acta 1832, 2257–2263.24012719

Lawrie SM , Buechel C , Whalley HC , Frith CD , Friston KJ , and Johnstone EC (2002). Reduced frontotemporal functional connectivity in schizophrenia associated with auditory hallucinations. Biol. Psychiatry 51, 1008–1011.12062886

Ma L , Skoblenick K , Seamans JK , and Everling S (2015). Ketamine-induced changes in the signal and noise of rule representation in working memory by lateral prefrontal neurons. J. Neurosci 35, 11612–11622.26290238

MacDonald AW (2008). Building a clinically relevant cognitive task: case study of the AX paradigm. Schizophr. Bull 34, 619–628.18487225

MacDonald AW , and Chafee MV (2006). Translational and developmental perspective on N-methyl-D-aspartate synaptic deficits in schizophrenia. Dev. Psychopathol 18, 853–876.17152404

MacDonald AW , Pogue-Geile MF , Johnson MK , and Carter CS (2003). A specific deficit in context processing in the unaffected siblings of patients with schizophrenia. Arch. Gen. Psychiatry 60, 57–65.12511173

MacDonald AW , Carter CS , Kerns JG , Ursu S , Barch DM , Holmes AJ , Stenger VA , and Cohen JD (2005). Specificity of prefrontal dysfunction and context processing deficits to schizophrenia in never-medicated patients with first-episode psychosis. Am. J. Psychiatry 162, 475–484.15741464

MacDonald ML , Alhassan J , Newman JT , Richard M , Gu H , Kelly RM , Sampson AR , Fish KN , Penzes P , Wills ZP , et al. (2017). Selective loss of smaller spines in schizophrenia. Am. J. Psychiatry 174, 586–594.28359200

Mitelman SA , Byne W , Kemether EM , Hazlett EA , and Buchsbaum MS (2005). Metabolic disconnection between the mediodorsal nucleus of the thalamus and cortical Brodmann's areas of the left hemisphere in schizophrenia. Am. J. Psychiatry 162, 1733–1735.16135634

Molina LA , Skelin I , and Gruber AJ (2014). Acute NMDA receptor antagonism disrupts synchronization of action potential firing in rat prefrontal cortex. PLoS One 9, e85842.24465743

Mukherjee P , Sabharwal A , Kotov R , Szekely A , Parsey R , Barch DM , and Mohanty A (2016). Disconnection between amygdala and medial prefrontal cortex in psychotic disorders. Schizophr. Bull 42, 1056–1067.26908926

Owen MJ , Sawa A , and Mortensen PB (2016). Schizophrenia. Lancet 388, 86–97.26777917

Panzeri S , Senatore R , Montemurro MA , and Petersen RS (2007). Correcting for the sampling bias problem in spike train information measures. J. Neurophysiol 98, 1064–1072.17615128

Perkel DH , Gerstein GL , and Moore GP (1967). Neuronal spike trains and stochastic point processes. II. Simultaneous spike trains. Biophys. J 7, 419–440.4292792

Pipa G , and Munk MH (2011). Higher order spike synchrony in prefrontal cortex during visual memory. Front. Comput. Neurosci 5, 23.21713065

Riehle A , Grün S , Diesmann M , and Aertsen A (1997). Spike synchronization and rate modulation differentially involved in motor cortical function. Science 278, 1950–1953.9395398

Scariati E , Padula MC , Schaer M , and Eliez S (2016). Long-range dys-connectivity in frontal and midline structures is associated to psychosis in 22q11.2 deletion syndrome. J. Neural. Transm. (Vienna) 123, 823–839.27094177

Schizophrenia Working Group of the Psychiatric Genomics Consortium (2014). Biological insights from 108 schizophrenia-associated genetic loci. Nature 511, 421–427.25056061

Schreiber T (2000). Measuring information transfer. Phys. Rev. Lett 85, 461–464.10991308

Schwarz E , Tost H , and Meyer-Lindenberg A (2016). Working memory genetics in schizophrenia and related disorders: an RDoC perspective. Am. J. Med. Genet. B Neuropsychiatr. Genet 171B, 121–131.26365198

Sekar A , Bialas AR , de Rivera H , Davis A , Hammond TR , Kamitaki N , Tooley K , Presumey J , Baum M , Van Doren V , et al. (2016). Schizophrenia risk from complex variation of complement component 4. Nature 530, 177–183.26814963

Shelton MA , Newman JT , Gu H , Sampson AR , Fish KN , MacDonald ML , Moyer CE , DiBitetto JV , Dorph-Petersen KA , Penzes P , et al. (2015). Loss of microtubule-associated protein 2 immunoreactivity linked to dendritic spine loss in schizophrenia. Biol. Psychiatry 78, 374–385.25818630

Sigurdsson T , Stark KL , Karayiorgou M , Gogos JA , and Gordon JA (2010). Impaired hippocampal-prefrontal synchrony in a genetic mouse model of schizophrenia. Nature 464, 763–767.20360742

Skoblenick K , and Everling S (2012). NMDA antagonist ketamine reduces task selectivity in macaque dorsolateral prefrontal neurons and impairs performance of randomly interleaved prosaccades and antisaccades. J. Neurosci 32, 12018–12027.22933786

Skoblenick K , and Everling S (2014). N-methyl-d-aspartate receptor antagonist ketamine impairs action-monitoring activity in the prefrontal cortex. J. Cogn. Neurosci 26, 577–592.24188365

Skoblenick KJ , Womelsdorf T , and Everling S (2016). Ketamine alters outcome-related local field potentials in monkey prefrontal cortex. Cereb. Cortex 26, 2743–2752.26045564

Stephan KE , Friston KJ , and Frith CD (2009). Dysconnection in schizophrenia: from abnormal synaptic plasticity to failures of self-monitoring. Schizophr. Bull 35, 509–527.19155345

Timms AE , Dorschner MO , Wechsler J , Choi KY , Kirkwood R , Girirajan S , Baker C , Eichler EE , Korvatska O , Roche KW , et al. (2013). Support for the N-methyl-D-aspartate receptor hypofunction hypothesis of schizophrenia from exome sequencing in multiplex families. JAMA Psychiatry 70, 582–590.23553203

Tu PC , Hsieh JC , Li CT , Bai YM , and Su TP (2012). Cortico-striatal disconnection within the cingulo-opercular network in schizophrenia revealed by intrinsic functional connectivity analysis: a resting fMRI study. Neuroimage 59, 238–247.21840407

Tu PC , Lee YC , Chen YS , Li CT , and Su TP (2013). Schizophrenia and the brain's control network: aberrant within- and between-network connectivity of the frontoparietal network in schizophrenia. Schizophr. Res 147, 339–347.23706416

Uhlhaas PJ , and Singer W (2015). Oscillations and neuronal dynamics in schizophrenia: the search for basic symptoms and translational opportunities. Biol. Psychiatry 77, 1001–1009.25676489

Umbricht D , Schmid L , Koller R , Vollenweider FX , Hell D , and Javitt DC (2000). Ketamine-induced deficits in auditory and visual context-dependent processing in healthy volunteers: implications for models of cognitive deficits in schizophrenia. Arch. Gen. Psychiatry 57, 1139–1147.11115327

Vicente R , Gollo LL , Mirasso CR , Fischer I , and Pipa G (2008). Dynamical relaying can yield zero time lag neuronal synchrony despite long conduction delays. Proc. Natl. Acad. Sci. USA 105, 17157–17162.18957544

Wang M , and Arnsten AF (2015). Contribution of NMDA receptors to dorsolateral prefrontal cortical networks in primates. Neurosci. Bull 31, 191–197.25754145

Wang M , Yang Y , Wang CJ , Gamo NJ , Jin LE , Mazer JA , Morrison JH , Wang XJ , and Arnsten AF (2013). NMDA receptors subserve persistent neuronal firing during working memory in dorsolateral prefrontal cortex. Neuron 77, 736–749.23439125

Wibral M , Pampu N , Priesemann V , Siebenhuhner F , Seiwert H , Lindner M , Lizier JT , and Vicente R (2013). Measuring information-transfer delays. PLoS One 8, e55809.23468850

Highlights

- Prefrontal rate-corrected spike correlation exhibits a prominent peak at 0-lag
- Blocking NMDAR reduces the strength of prefrontal 0-lag spike correlation
- Reduced 0-lag correlation is accompanied by functional decoupling of PFC circuits
- A spike-timing defect caused by NMDR malfunction could disconnect PFC circuits

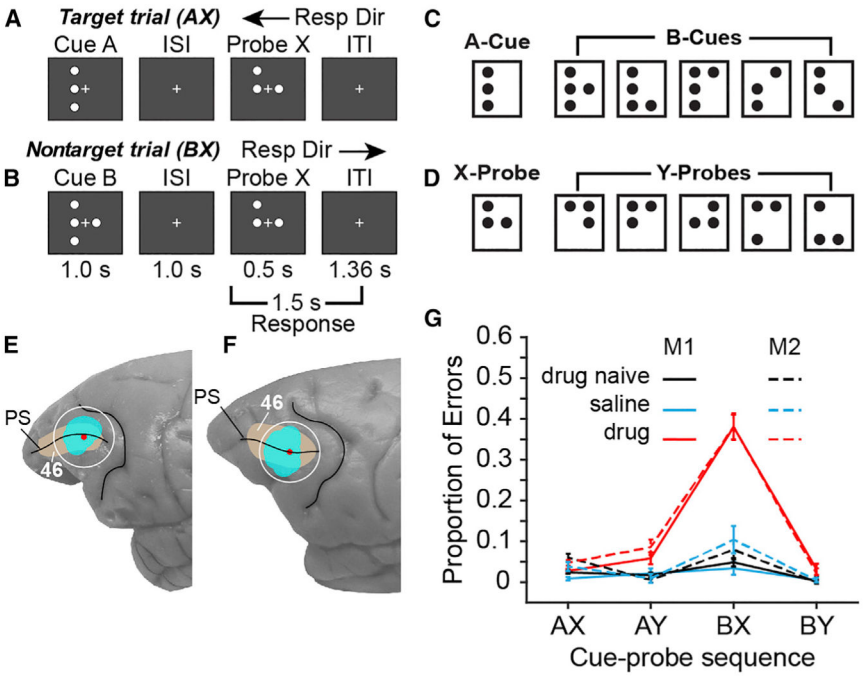

Figure 1. DPX Task, Recording Locations, and Task Performance

(A and B) Event sequence in the DPX task. A cue and a probe stimulus are displayed each trial. (A) On AX trials, the A-cue is followed by the X-probe. This is the target sequence, and the monkey is rewarded for moving the joystick to the left (target response) following probe onset. (B) On BX trials, the B-cue stored in working memory must override the habitual target response to the X-probe to produce the correct nontarget response to the X-probe in this context.

(C) Cue stimuli. One dot pattern was designated the A-cue, and five dot patterns were collectively designated B-cues.

(D) Probe stimuli. One dot pattern was designated the X-probe, and five dot patterns were collectively designated Y-probes.

(E and F) Locations of ensemble neural recording (cyan) in Brodmann area 46 (tan) surrounding the principal sulcus (PS) in monkeys 1 (E) and 2 (F). Red dots indicate the centers of the recording chambers. (G) Behavioral performance on the DPX task while the neural data described in this report was recorded. The y axis indicates the proportion of errors (±2 SE above and below the mean) committed during DPX task performance separated by cue-probe sequence (trial type) and experimental condition in monkeys 1 (solid) and 2 (dashed).

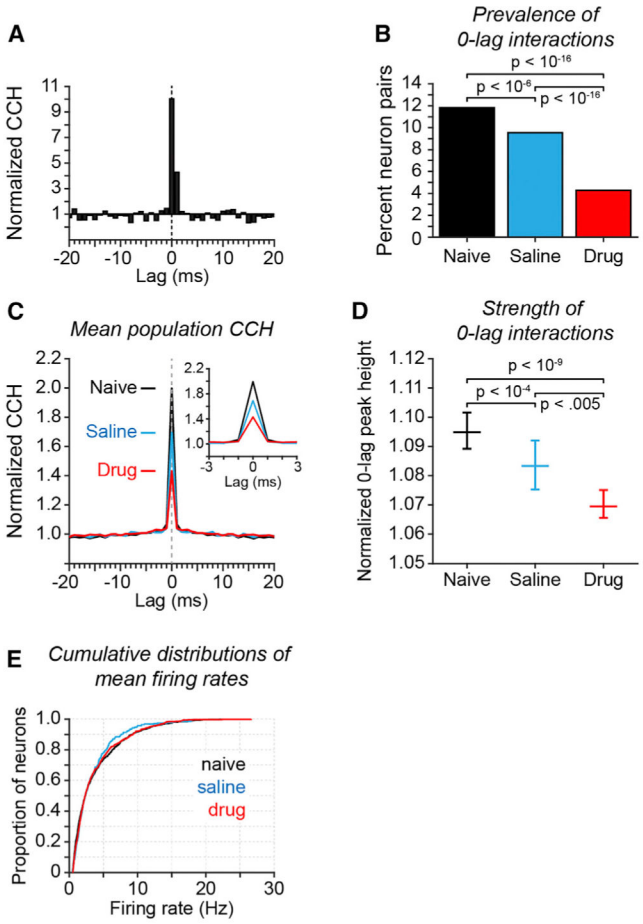

Figure 2. Influence of NMDAR Antagonist on Spike Synchrony in Prefrontal Cortex

Results of cross-correlation analysis applied to the spike trains of pairs of simultaneously recorded prefrontal neurons. Experimental condition is indicated by color (B-E): drug-naive (black), saline (blue), and drug (red).

(A) Example CCH of a neuron pair recorded in the drug-naive condition with a significant CCH peak at 0-lag. The CCH is normalized by dividing counts in each bin in the original data by the mean count of the bootstrap distribution of spike-jittered CCHs at that bin.

(B) Proportion of all neuron pairs recorded that exhibited a significant peak at 0-lag (±1 ms). A neuron pair was considered to exhibit a significant 0-lag CCH peak if the sum of the counts of joint spikes at lags − 1,0, and +1 exceeded the 99th percentile of the distribution of corresponding sums computed from the spike-jittered CCHs. p values reflect significance of differences in proportion of significantly coupled neuron pairs across experimental conditions (Fisher's exact test; n = 1,736/14,674, 469/4,908, and 518/12,112 significant pairs out of total for naive, saline, and drug, respectively).

(C) Mean population CCHs separated by experimental condition (insert shows the 0-lag peak of the same data on an expanded ±3 ms lag timescale). All recorded neuron pairs were included. CCH normalization as in (A).

(D) Median 0-lag CCH peak height as a function of experimental condition. For each neuron pair, 0-lag peak height was computed as the sum of joint spike counts in the −1, 0, and +1 lag bins of the original data and was normalized by dividing by the mean of the sum of

counts in the same bins of the spike-jittered CCHs. Data plotted reflects the median of the distribution of normalized 0-lag peak heights across all recorded neuron pairs in each experimental condition (error bars reflect 95% confidence intervals of the median; p values calculated by Kruskal-Wallis test followed by Tukey's HSD test).

(E) Cumulative distributions of mean firing rate by experimental condition. No significant differences in mean firing rate were found (Kruskal-Wallis test; saline versus drug, $p = 0.99$; naive versus drug, $p = 0.90$, saline versus drug $p = 0.97$).

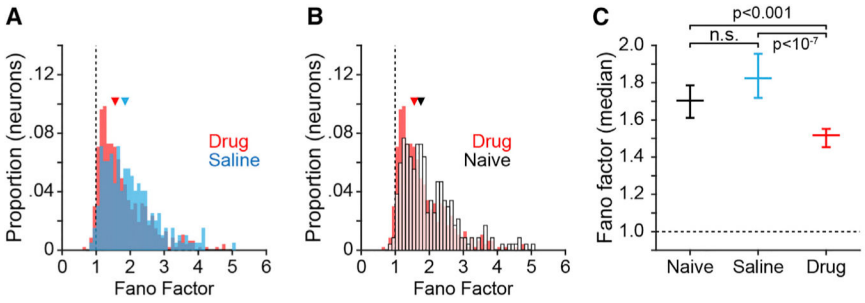

Figure 3. Influence of NMDAR Antagonists on Spike Timing Variability in Prefrontal Cortex

To quantify variability in spike timing we computed the Fano factor as the variance in spike counts over a sequence of 50-ms bins divided by the mean firing rate on a per-neuron basis. (A and B) Frequency distribution of individual neuron Fano factor values for drug and saline (A), and drug and drug-naive (B) conditions. Vertical dashed lines in (A) and (B) indicate a Fano factor of 1, triangles represent the median of each distribution.

(C) Median Fano factor (error bars indicate 95% confidence intervals) by experimental condition; p values calculated by Kruskall-Wallis test followed by Tukey's HSD test.

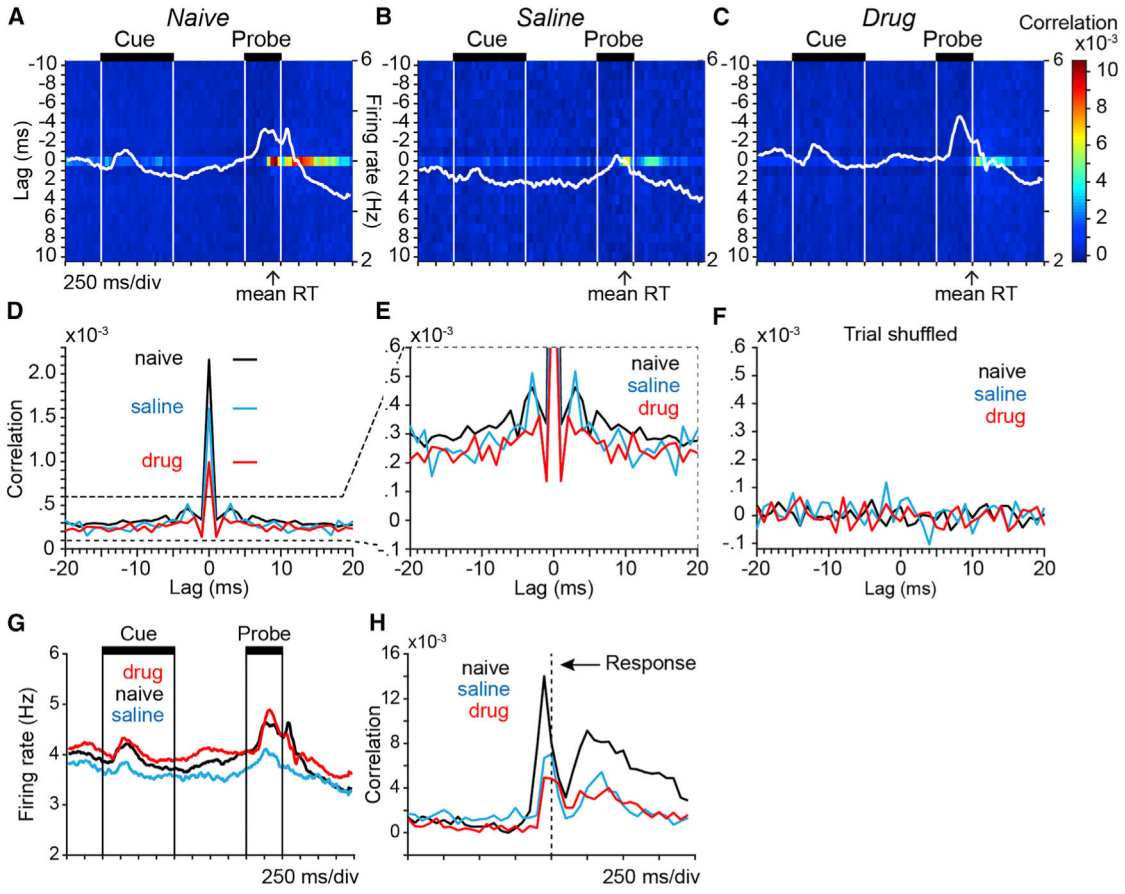

Figure 4. Spike Correlation at 0-Lag Was Strongly Modulated in Time throughout the Trial

Heatmaps plot the population average spike correlation between pairs of simultaneously recorded prefrontal neurons as a function of lag between spikes in the two neurons (vertical axis; 1-ms resolution) and time within the DPX trial (horizontal axis; 50-ms resolution). Data in all panels were restricted to AX trials. Spike times were aligned to cue onset and data from all simultaneously recorded pairs of neurons were included.

(A–C) Average population spike correlation in the drug-naive (A), saline (B), and drug (C) conditions. Spike density functions (white lines) superimposed on each panel illustrate concurrent modulation in population firing rate (firing rate scales at right). Arrows under each panel indicate mean reaction time (RT) in each experimental condition.

(D) Population average spike correlation averaged across time in the trial at spike lags from −20 to +20 ms and plotted separately by experimental condition. Horizontal lines indicate the heights of the 0-lag peaks of corresponding color.

(E) Same data as in (D) but plotted on an expanded y axis to better illustrate spike correlation at flanking non-zero lags.

(F) Population average spike correlation computed using trial-shuffled spike trains from the same neuronal pairs as in (D).

(G) Population average spike density functions illustrate modulation in population firing rate of the same neurons contributing to the correlation analysis throughout the DPX trial plotted separately by experimental condition.

(H) Time course of population average 0-lag spike correlation in pairs of prefrontal neurons using spike train data aligned to the time of the motor response (vertical dashed line).

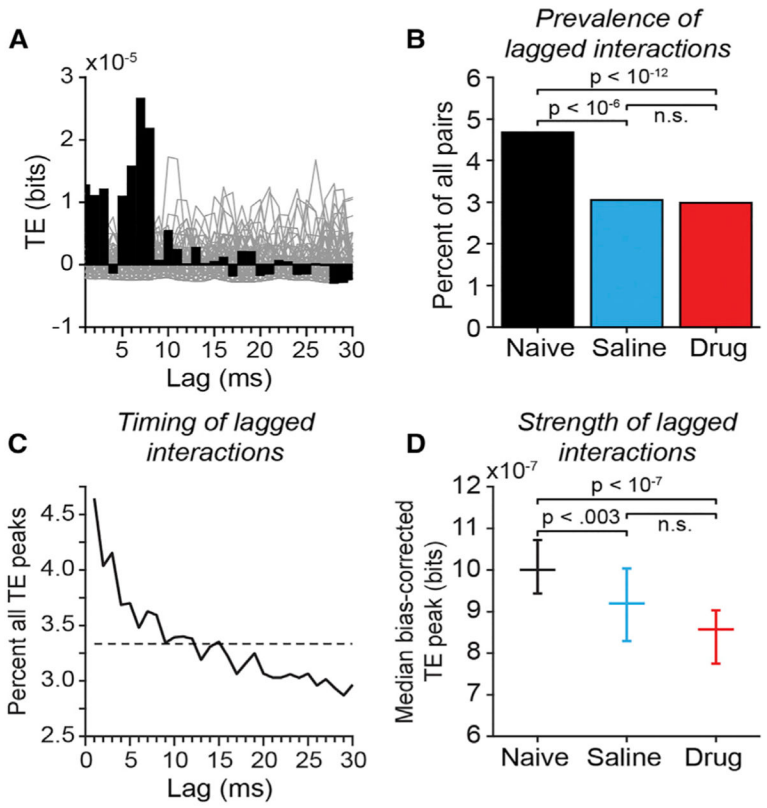

Figure 5. Transfer Entropy in Pairs of Simultaneously Recorded Prefrontal Neurons

(A) Example bias-corrected transfer entropy (TE) function for a pair of prefrontal neurons recorded in the drug-Naive condition. For each neuron pair, TE values (black bars) in each lag bin were bias corrected by subtracting the mean at the corresponding lag bin of a bootstrap distribution of TE values obtained from the same neurons after randomly jittering all spike times within a± 30 ms window to destroy the temporal relationship between the spike trains (gray lines plot TE functions computed from spike jittered data).

(B) The proportion of all neuronal pairs recorded that were identified as significantly coupled by TE analysis separated by experimental condition. Neuron pairs were considered significantly coupled if the peak of the TE time course exceeded the 99.9th percentile of peaks in any lag bin in 1000 spike-jittered bootstrap iterations of the analysis. Neuron pairs (coupled/all): drug-naive: 677/14,468 pairs; saline: 150/4,914 pairs; drug: 365/12,230 pairs. p values reflecting the significance of differences between experimental conditions were calculated using Fisher's exact test.

(C) Distribution of time bins (lags) in which peak TE values occurred, across all neuron pairs. Dashed line indicates the expected values if peak locations were uniformly distributed across lags.

(D) Median bias-corrected peak TE values across all neuron pairs (error bars reflect 95% confidence intervals of the median); p values reflecting the significance of differences between experimental conditions were calculated using the Kruskall-Wallis test followed by Tukey's HSD test.

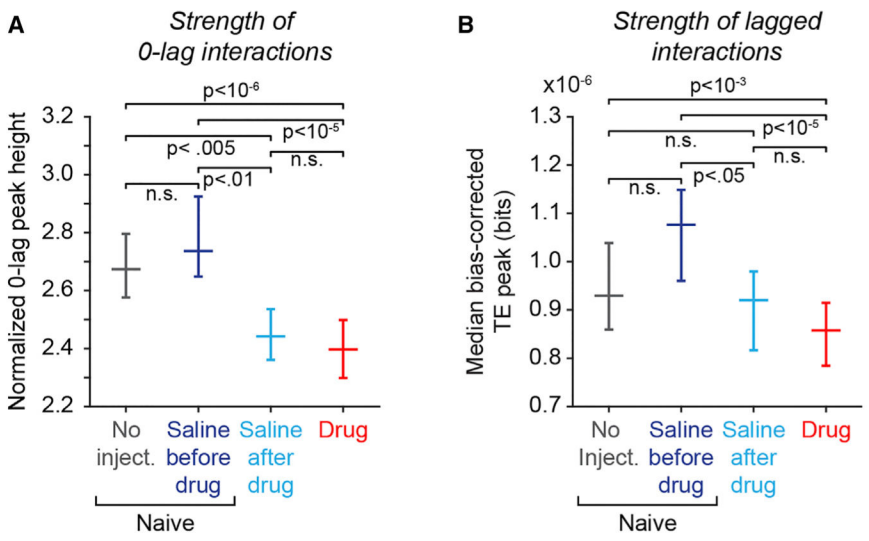

Figure 6. Periodic Exposure to NMDAR Antagonists Is Associated with Persistent Reduction in Both 0-Lag Spike Synchrony and Lagged Functional Interactions in Prefrontal Networks

Comparison of 0-lag CCH and lagged TE functional coupling metrics between days when no injection was given before first drug exposure ("No Inject.," gray), days when saline was injected before first drug exposure ("Saline before drug," dark blue), days when saline was injected after first drug exposure ("Saline after drug," light blue), and days that PCP was injected ("Drug," red). "No inject." and "Saline before drug" data together comprise the "Naive" experimental condition in Figures 1, 2, 3, 4, and 5. p values reflecting the significance of differences between experimental conditions were calculated using the Kruskal-Wallis test followed by Tukey's HSD test ("n.s." indicates $p > 0.05$, not significant).

(A) Median normalized 0-lag CCH peak height as a function of experimental condition (data restricted to pairs with significant 0-lag peaks; error bars reflect 95% confidence intervals of the median). Number of neuron pairs: "No injection" = 1,099; "Saline before drug" = 637; "Saline after drug" = 469; "Drug" = 518.

(B) Median bias-corrected nonzero lag TE peak height as a function of experimental condition. (All neuronal pairs included in the TE analysis to increase the power to detect differences between experimental conditions). Number of neuron pairs: "No injection" = 6,762; "Saline before drug" = 7,706; "Saline after drug" = 4,914; "Drug" = 12,230.

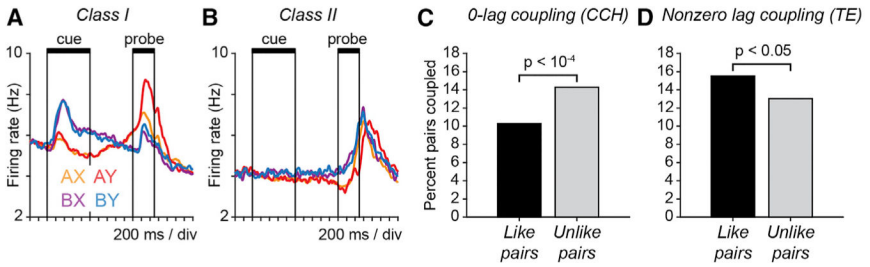

Figure 7. Patterns of Functional Coupling between Neurons Reflect the Physiological Signals They Generate during Behavior

(A and B) Average population activity of class I (A) and class II (B) neurons defined by their patterns of task-related activity during the DPX task. (See STAR Methods for statistical criteria defining class I and II neurons.) Population spike density functions of different colors illustrate firing rate over time on subsets of trials separated by cue-probe sequence (AX, AY, BX, and BY). (A) Class I (39% of recorded neurons): on B-cue trials, class I neurons exhibit a strong response to the cue. On A-cue trials, class I neurons exhibit a ramping of activity that peaks in the probe period. (B) Class II (14% of recorded neurons): neurons in class II do not exhibit a strong response to the cue (differentiating them from class I neurons). Rather they exhibit a ramping of activity during the probe period that is greater on B-cue than A-cue trials.

(C and D) Relation between neuronal pair type and functional coupling. Neuron pairs in this analysis were restricted to those in which both neurons exhibited task-related activity and were assigned either to class I or II. “Like pairs” were defined as those in which the two neurons belonged to the same physiological class (either both neurons in class I or II). “Unlike pairs” were defined as those in which one neuron belonged to class I and the other to class II. Bars indicate the percent of all recorded like neuron pairs (black) and unlike neuron pairs (gray) that were significantly coupled either (C) at 0-lag (CCH) or (D) at nonzero lag (TE). p values indicate the significance of the difference in proportions (Fisher’s exact test). (C) Percent of recorded like pairs (black; n = 3,324) and unlike pairs (gray; n = 1,729) that were significantly coupled at 0-lag by CCH analysis. (D) Percent of recorded like pairs (black; n = 3,424) and unlike pairs (gray; n = 1,757) that were significantly coupled at nonzero lag by TE analysis.

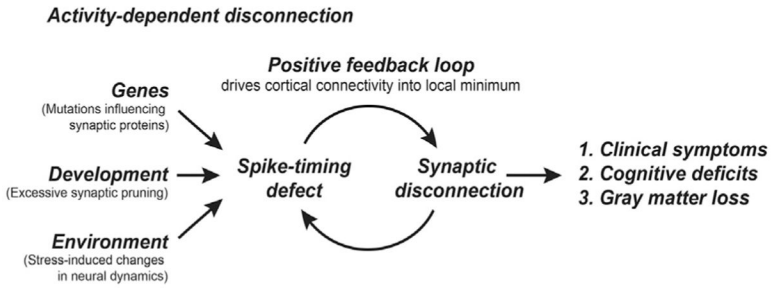

Figure 8. Spike-Timing-Dependent Synaptic Disconnection in Schizophrenia

In this theory, multiple insults that increase risk for schizophrenia converge on a common effect that is to reduce synchronous and near-synchronous spiking in cortical networks, preferentially but not exclusively impacting prefrontal cortical networks. These insults include: (1) SNPs identified in GWAS studies that are likely to modify the function or expression of synaptic proteins that mediate or modulate NMDAR synaptic transmission, (2) developmental events that include normal synaptic pruning in adolescence, which may be accelerated by risk mutations in schizophrenia, and (3) environmental factors, such as stress, that might influence oscillatory rhythms in cortical networks or other aspects of neural system dynamics that influence spike timing. The reduction in synchronous spiking downstream of these insults then drives synaptic disconnection of prefrontal cortical networks via spike-timing plasticity mechanisms. Clinical symptoms and cognitive deficits seen in schizophrenia emerge largely as a consequence of the eventual disconnection of prefrontal cortical networks. Loss of synaptic connectivity contributes to the progressive loss of cortical gray matter volume, particularly affecting prefrontal cortex.

KEY RESOURCES TABLE

REAGENT or RESOURCE	SOURCE	IDENTIFIER
Chemicals, Peptides, and Recombinant Proteins		
Phencyclidine hydrochloride	Sigma-Aldrich	P3029
Experimental Models: Organisms/Strains		
Rhesus macaque (Macaca mulatta)	N/A	N/A
Software and Algorithms		
MATLAB	MathWorks	RRID:SCR_001622
Transfer entropy toolbox	Ito et al., 2011	https://code.google.com/archive/p/transfer-entropy-toolbox/